Electronic Supplementary Information (ESI)

Porous Calcium-Manganese Oxide Microspheres for Electrocatalytic Oxygen Reduction with High Activity

Xiaopeng Han,[a] Tianran Zhang,[a] Jing Du,[a] Fangyi Cheng*[,a,b] and Jun Chen*[,a,b]

[a]Institute of New Energy Material Chemistry and [b]Key Laboratory of Advanced Energy Materials Chemistry (Ministry of Education), College of Chemistry, Nankai University, Tianjin, 300071, China. Fax: 86-22-23506808; Tel: 86-22-23506808; E-mail: fycheng@nankai.edu.cn, chenabc@nankai.edu.cn

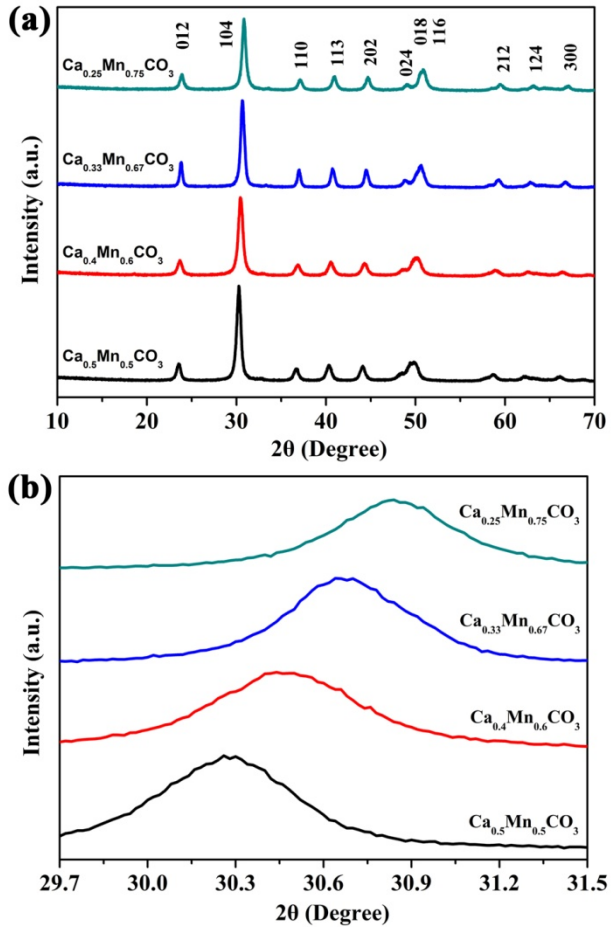

Fig S1. (a) Powder XRD patterns of the $Ca_xMn_{1-x}CO_3$ precursors and (b) the enlargement of the strongest reflection peaks. The absence of well defined and incipient superstructure reflections indicated that the precipitated carbonate precursors were single-phase intermediate members of calcite-rhodochrosite $Ca_xMn_{1-x}CO_3$ solid-solutions.[s1] Furthermore, the diffraction peaks of these carbonates were shifted to higher 2θ angles with increasing Mn-content, as observed in the enlarged XRD patterns (Fig. 2b). This shift was indicative of a shrunk crystal lattice due to the substitution of Ca^{2+} by Mn^{2+} that has a shorter ionic radius (0.80 versus 0.99 Å).

The typical synthesis of solid-solution carbonate precursors is described as follows. First, $MnCO_3$ and $CaCO_3$ were precipitated separately from $Mn(NO_3)_2$ and $Ca(NO_3)_2$ solution with a large excess of NH_4HCO_3 and $(NH_4)_2CO_3$, respectively. The

carbonate precipitates were washed repeatedly with distilled water and vacuum-dried at 100 °C. After dissolving $CaCO_3$ and $MnCO_3$ in dilute nitric acid, an aqueous solution containing the desired amounts of calcium and manganese was added to an aqueous solution containing excess $(NH_4)_2CO_3$ under vigorous stirring. The resulting precipitate was collected as the precursor, which was stored in an inert atmosphere to prevent any premature oxidation.

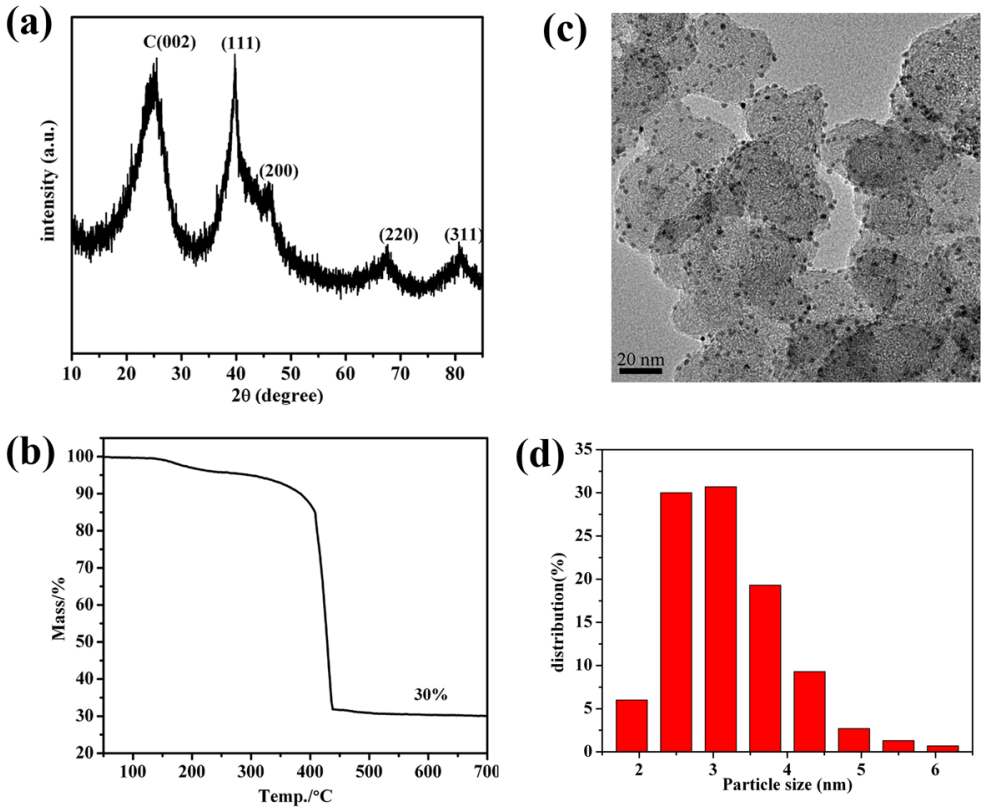

Fig S2. Characterization of the as-prepared Pt/C benchmark: (a) XRD pattern, (b) thermogravimetry curves measured in air, indicating the Pt loading is around 30 wt%, (c) TEM image and (d) the corresponding distribution of Pt particle size. Thermogravimetry analysis was carried out with a NETZSCH TG 449 analyzer at an O_2 atmosphere and a heating rate of 10 °C min^{-1}.

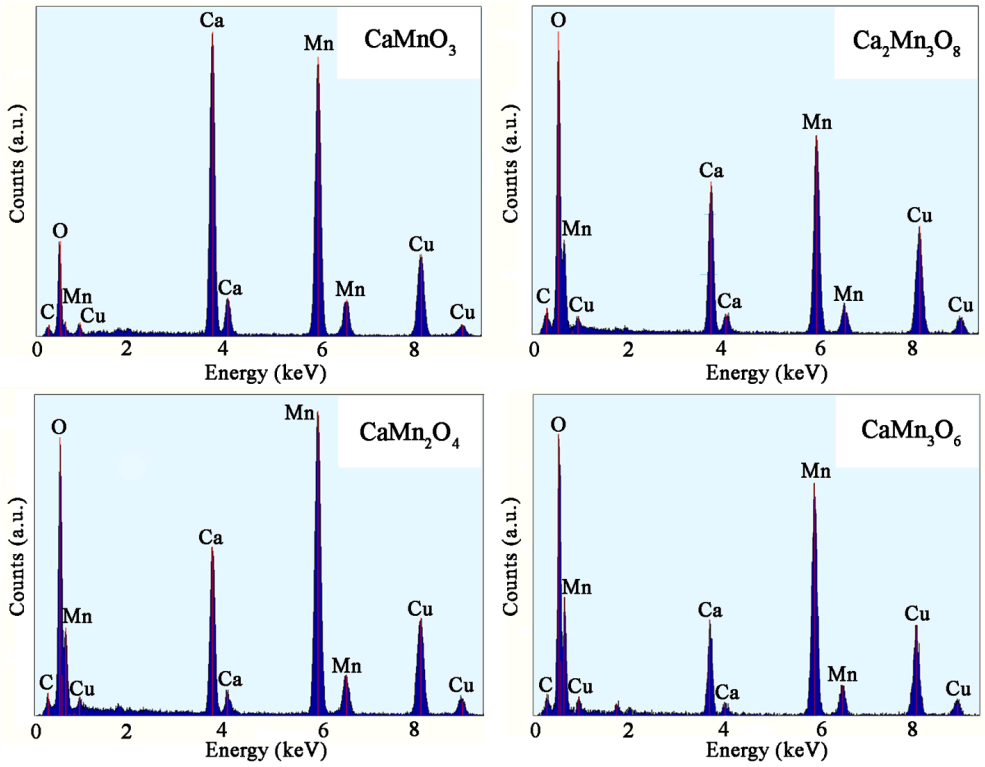

Fig S3. EDX spectra of the synthesized Ca-Mn-O compounds.

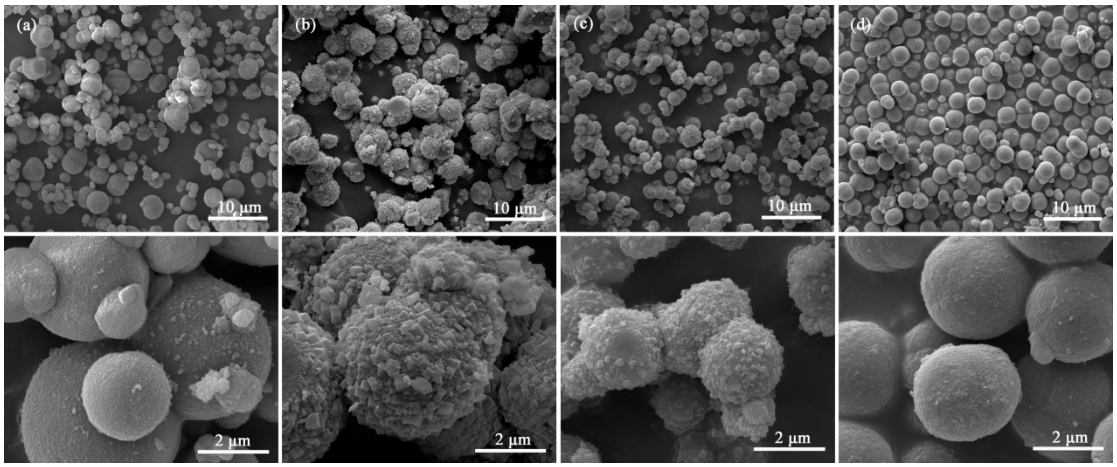

Fig S4. SEM images of carbonate precursors (a) $Ca_{0.5}Mn_{0.5}CO_3$, (b) $Ca_{0.4}Mn_{0.6}CO_3$, (c) $Ca_{0.33}Mn_{0.67}CO_3$, and (d) $Ca_{0.25}Mn_{0.75}CO_3$.

The theoretical densities (estimated from crystal structures) of typical carbonates and Ca-Mn-O oxides are as follows: $CaCO_3$, 2.71 g cm^{-3}; $Ca_{05}Mn_{0.5}CO_3$, 3.18 g cm^{-3}; $MnCO_3$, 3.71 g cm^{-3}; $CaMnO_3$, 4.59 g cm^{-3}; $Ca_2Mn_3O_8$, 4.13 g cm^{-3}; $CaMn_2O_4$, 4.6 g cm^{-3}; $CaMn_3O_6$, 4.66 g cm^{-3}. We suggest that the difference in crystal densities between the carbonate precursors and the oxides is one of the main reasons for the formation of porous microstructures after thermal decomposition of the precursors.

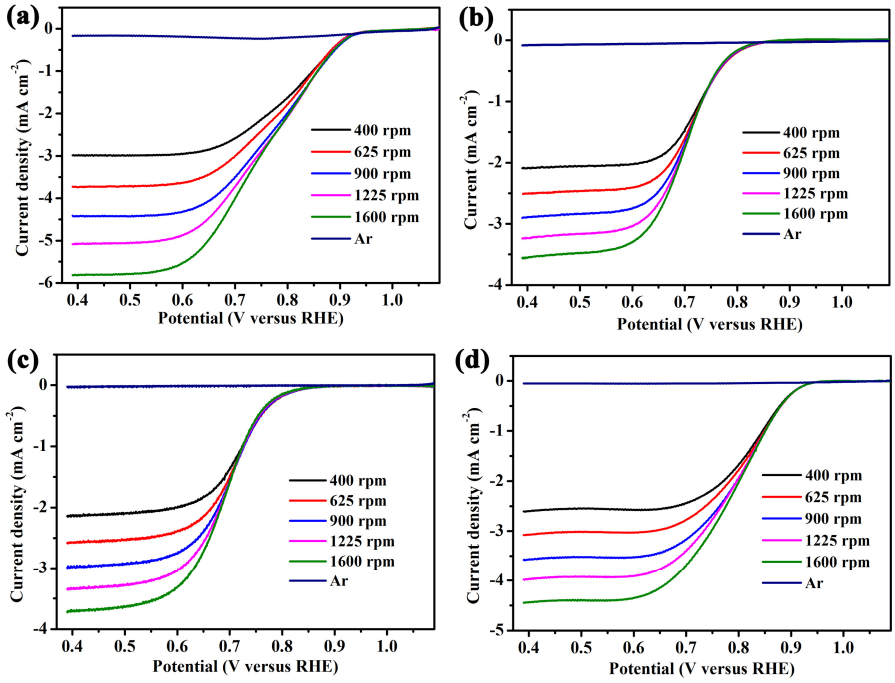

Fig S5. LSVs of (a) $CaMnO_3$, (b) $Ca_2Mn_3O_8$, (c) $CaMn_2O_4$ and (d) $CaMn_3O_6$ samples recorded in Ar- and O_2-saturated 0.1 M KOH solution.

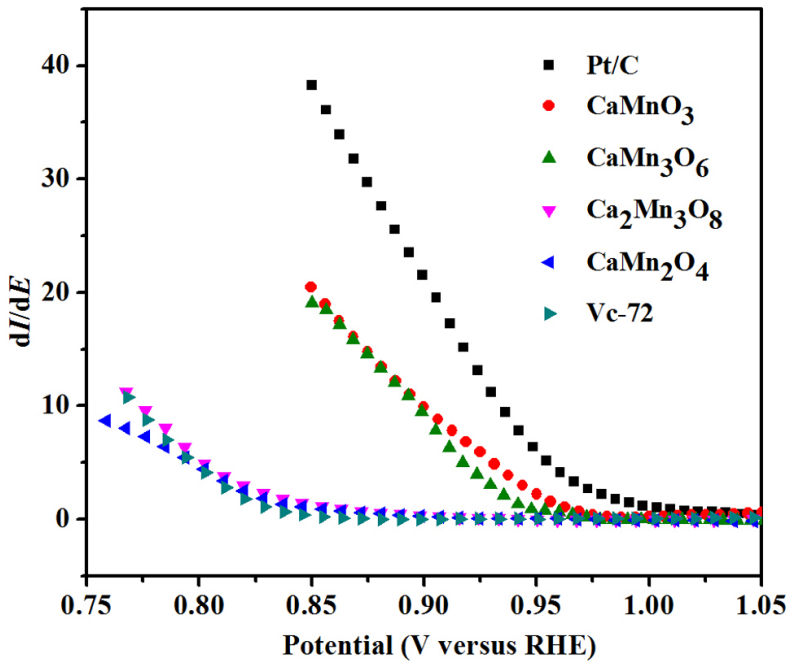

Fig S6. The differential plots of *I* versus *E* constructed from the LSV curve. From the sharply increased slope of the plots, the onset potential indicative of the start of the ORR can be clearly seen.

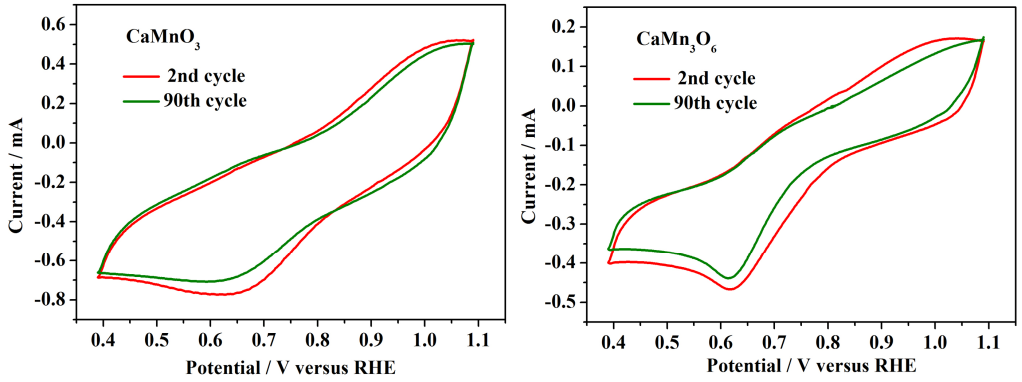

Fig S7. Cyclic voltammograms of $CaMnO_3$ and $CaMn_3O_6$ supported in GC electrode in O_2-saturated 0.1 M KOH solution at a scan rate of 100 mV s^{-1}. Elemental analysis (both atomic emission and absorption spectroscopies) showed negligible leaching of Ca and Mn cations in the electrolytes after repeated cycles.

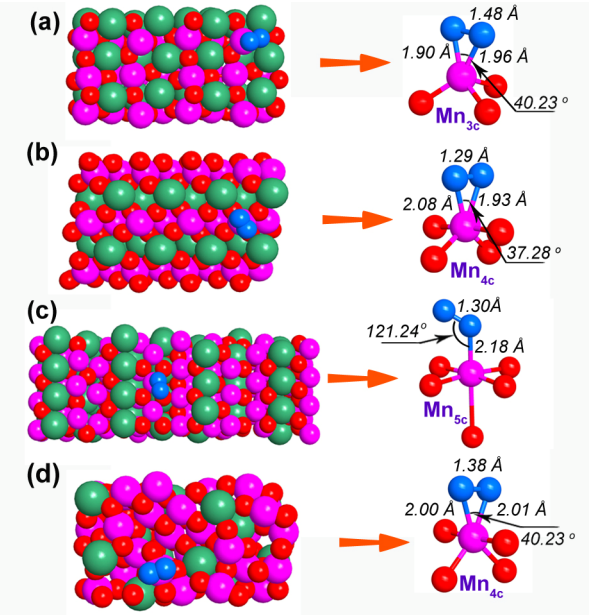

Fig S8. Computational configuration of oxygen adsorption on surfaces of (a) $CaMnO_3$, (b) $Ca_2Mn_3O_8$, (c) $CaMn_2O_4$ and (d) $CaMn_3O_6$. Green, pink, red and blue represent Ca, Mn, lattice O and adsorbed O, respectively. For $CaMnO_3$, $Ca_2Mn_3O_8$ and $CaMn_3O_6$, molecular oxygen is bound to the coordination-unsaturated surface Mn cations through a lateral Griffith (side-on) manner, favoring the rupture of the O-O bond and the 4e ORR pathway.[s2,s3] In comparison, the $CaMn_2O_4$ surface binds oxygen via a Pauling (end-on) form, which is advantageous to the 2e reduction.[s2,s3] The bond length of adsorbed oxygen molecules can be viewed as a descriptor to evaluate the interaction between oxygen and catalyst surfaces. Upon adsorption, all the O-O bonds are longer relative to that in vacuum (1.24 Å), indicating the activation of O_2. Notably, the degree of O-O elongation by the oxide catalysts coincides with the order of their catalytic activities. The different manner and strength of oxygen binding on the series Ca-Mn-O compounds result from the difference in the surface valence of Mn and the crystal structures. Further computational investigation is underway to include more extensive analysis such as electronic structure, binding energy, and reaction pathways.

Computational Details: All calculations were performed by the Vienna ab initio simulation package (VASP) using periodic density functional theory (DFT).[s4] Generalized gradient approximation (GGA) of Perdew–Wang 1991 (PW91) was supplemented by the rotationally invariant " +U " description by Dudarev et al.[s5] Projector augmented wave (PAW) method was employ to describe valence-electron interactions.[s6] Energy cutoff was set to 400 eV and electron smearing was employed using Gaussian smearing technique with a width of 0.2 eV. The Hubbard U value of Mn atoms was chosen to be 4.5 eV according to previous reports.[s7,s8] Spin polarization calculation was carried out for all possible structures with the bottom two layers of the surface fixed. The lattice parameters of the four Ca-Mn-O compounds were referred to experimental values. To investigate oxygen adsorption, surface models with 10.4 Å of a vacuum layer were used. The most stable surfaces were referred to the XRD analysis: (121) for $CaMnO_3$, (020) for $Ca_2Mn_3O_8$, (021) for $CaMn_3O_6$, and (023) for $CaMn_2O_4$. Electronic energies were computed with the SCF tolerance of 10^{-5} eV and total forces were converged to less than 0.02 eV/Å.

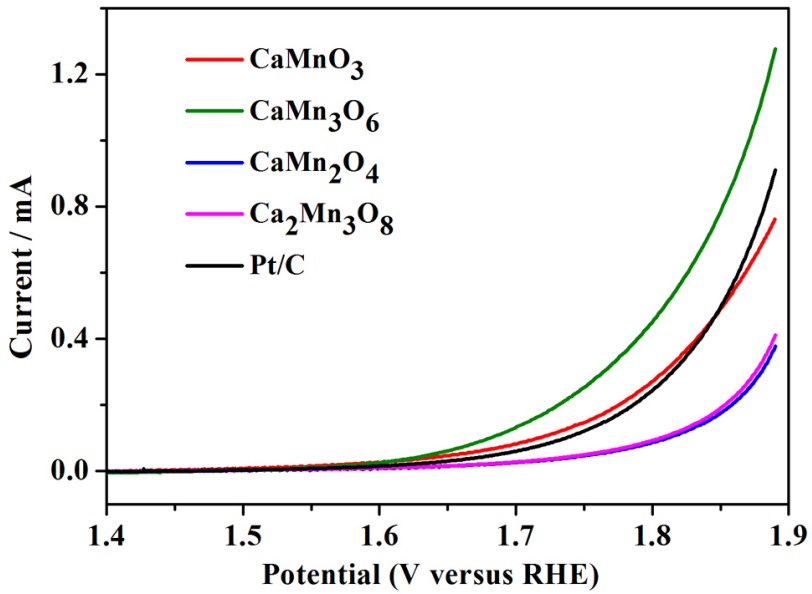

Fig S9. The OER activities of the synthesized Ca-Mn-O microspheres and the comparative Pt/C.

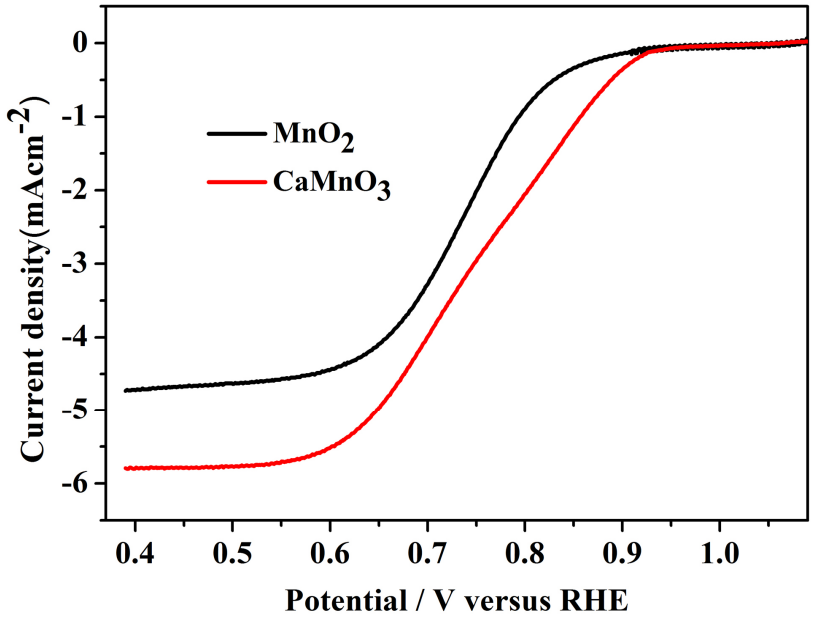

Fig S10. The ORR activities of β-MnO_2 and $CaMnO_3$.

Supplemental References:

s1. D. Katsikopoulos, Á. Fernández-González and M. Prieto, *Geochim. Cosmochim. Acta*, 2009, **73**, 6147.

s2. E. Yeager, *Electrochim. Acta*, 1984, **29**, 1527.

s3. W. Vielstich, A. Lamm and H. A. Gasteiger, *Handbook of Fuel Cells – Fundamentals, Technology and Applications*, Wiley, Chichester, 2003.

s4. G. Kresse and J. Furthmüller, *Phys. Rev. B*, 1996, **54**, 11169.

s5. S. L. Dudarev, G. A. Botton, S. Y. Savrasov, C. J. Humphreys and A. P. Sutton, *Phys. Rev. B*, 1998, **57**, 1505.

s6. P. E. Blöchl, *Phys. Rev. B*, 1994, **50**, 17953.

s7. C. Franchini, R. Podloucky, J. Paier, M. Marsman and G. Kresse, *Phys. Rev. B*, 2007, **75**, 195128.

s8. G. Trimarchi and N. Binggeli, *Phys. Rev. B*, 2005, **71**, 035101.